Soil Dynamics and Earthquake Engineering 47 (2013) 83–91

Contents lists available at SciVerse ScienceDirect

Soil Dynamics and Earthquake Engineering

journal homepage: www.elsevier.com/locate/soildyn

Nonlinear rocking stiffness of foundations

G. Gazetas *, I. Anastasopoulos, O. Adamidis, Th. Kontoroupi

Laboratory of Soil Mechanics, National Technical University of Athens, Greece

ARTICLE INFO

Article history:
Received 18 February 2012
Received in revised form
5 December 2012
Accepted 20 December 2012
Available online 23 January 2013

ABSTRACT

The response of surface foundations to large overturning moments is studied under undrained conditions. Rigid circular, strip, and rectangular footings of various aspect ratios are considered, with the soil modeled as an inelastic homogeneous deposit, characterized by an elastic (small-strain) shear modulus G_o, an undrained shear strength S_u, and a G/G_o versus γ curve appropriate for medium-plasticity clays. Three stages of foundation performance, ranging from the initial elastic fully-bonded response, to the nearly-elastic but nonlinear response with the foundation partially detaching and uplifting from the soil, and finally to the ultimate stage where full mobilization of soil bearing failure mechanisms develop. Simple to use formulas or charts are developed for all stages of response in terms of dimensionless parameters, prominent among which is the static factor of safety against bearing-capacity failure under purely-vertical loading.

1. Introduction

Research on seismic soil–structure interaction (SSI) over the last decades has mostly relied on the assumption of linear (or at most equivalent-linear) elastic soil behavior and fully bonded contact between footing and soil (examples: [30,31,36,48,49,52,54]). Seismic design of structure–foundation systems has followed a somewhat parallel path: the still prevailing "capacity design" philosophy allows substantial plastic deformation in the superstructure but requires no significant yielding developed below ground level. This requirement implies that:

- foundation elements (e.g. piles, footings, caissons) will remain structurally elastic (or nearly elastic);
- bearing capacity soil failure mechanisms will not be mobilized;
- sliding at the soil–foundation interface will not take place, while the amount of foundation uplift will be limited to not more than about half of the contact area.

However, seismic motions recorded in the last 20 years, starting with the earthquakes of Northridge (1994) and Kobe (1995), have revealed that very large ground and spectral acceleration levels can be experienced in near-fault zones. Seismic loads transmitted onto shallow foundations in such cases will most probably induce significant nonlinear inelastic action in the soil and soil–foundation interface. Among the most spectacular examples of strongly-nonlinear foundation response which led to bearing capacity and uplifting failures of buildings are from the city of Adapazari during the Kocaeli 1999 earthquake [17]. Although these failures had been initially attributed to soil liquefaction, subsequent studies suggested the development of bearing capacity failure mechanisms passing through the very soft silt as the main culprit. The need for considering soil nonlinearity in (re)designing foundations as part of a rehabilitation scheme has long been recognized in normative documents (see FEMA [12]). Thus, in the last 15 years or so numerous publications have dealt with soil and foundation inelasticity [2–9,11–14,17–20,22,26,28,34,35,37–39,42–46,51].

The scope of this paper is to present results for the nonlinear static rocking stiffness of foundations having various plan shapes (strip, square, circle, rectangle), supported on a uniform layer of undrained clay (Fig. 1). Finite element analyses are performed to this end. Both geometric nonlinearity (a consequence of detachment of the footing from the soil), and material inelasticity (due to declining soil modulus at strains exceeding about 0.01% and eventually to soil failure, controlled by S_u) are properly reflected in the analyses. The results are given in the form of formulae and graphs that can be readily (even if iteratively) used in equivalent linear analyses and in displacement-based design.

2. Method of analysis

A series of two- and three-dimensional (2D, 3D) finite element analyses have been performed using ABAQUS [1]. The soil is a saturated homogeneous clay responding in undrained fashion with a shear strength S_u and maximum shear modulus G_{max}. The

* Corresponding author.
E-mail address: gazetas@ath.forthnet.gr (G. Gazetas).

0267-7261/$ - see front matter © 2013 Elsevier Ltd. All rights reserved.
http://dx.doi.org/10.1016/j.soildyn.2012.12.011

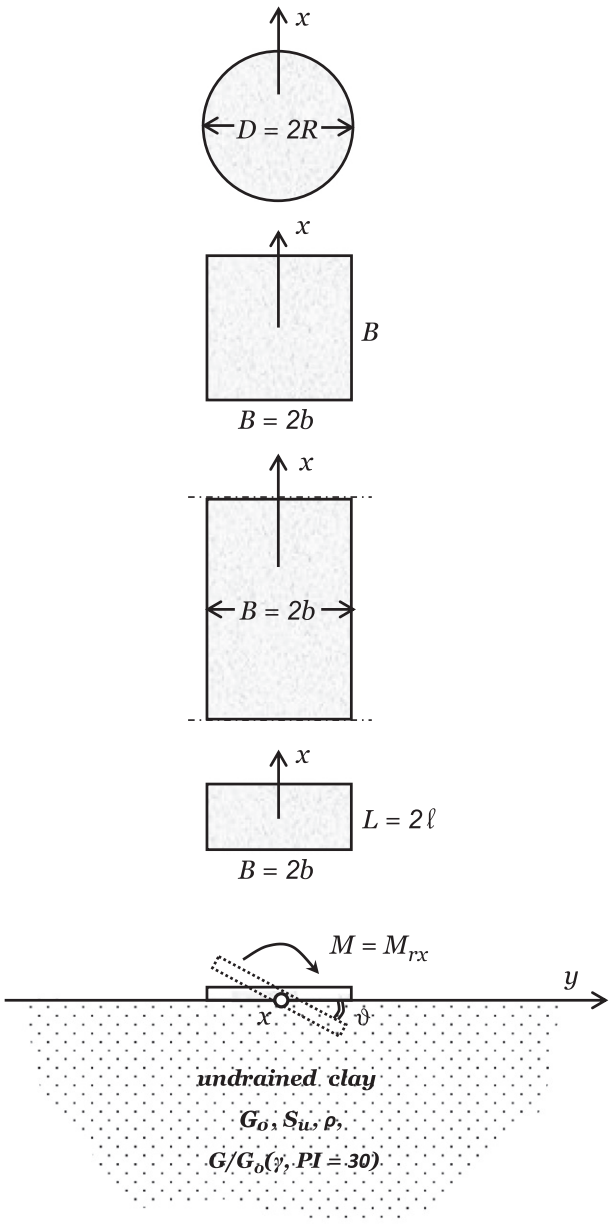

Fig. 1. The four geometries in plan and a (single) cross-section.

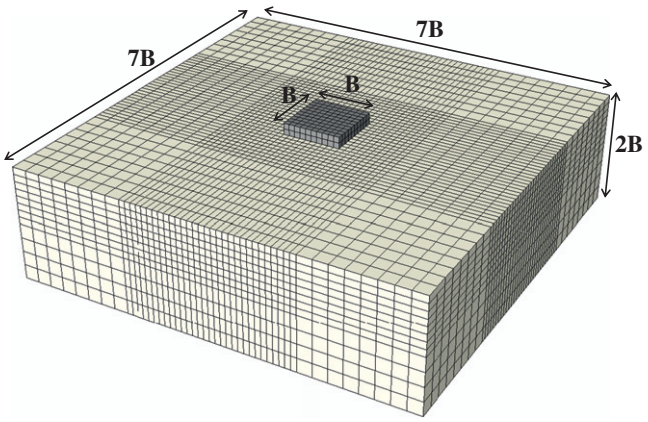

Fig. 2. 3-D view of typical finite element mesh: square foundation.

footing, of width B in the direction perpendicular to the axis of rotation, is structurally absolutely rigid. Except for the special case of plane strain (for which 4-noded plane strain elements are used), the soil is modeled with 8-noded cubic elements, as shown in Fig. 2. We have used fully integrated first-order isoparametric elements, in which the volume changes at Gauss points are replaced by the average volume change of the element. This technique, also known as selective reduced-integration (because the order of integration is reduced in selected terms), helps to prevent mesh locking, providing accurate solutions in (nearly) incompressible materials.

An advanced tensionless contact algorithm has been adopted to simulate the potential separation and uplifting of the foundation from the soil: interface elements allow the nodes to be in contact (when closed) or separated (when open). To achieve a reasonably stable time increment without jeopardizing the accuracy of the analysis, we modified the default hard contact pressure–overclosure relationship of ABAQUS with a suitable exponential relationship. A large coefficient of friction at the soil–footing interface was chosen deliberately to prevent gross sliding of the footing on the ground. This assumption was deemed necessary in order to avoid "parasitic" sliding displacements, aiming to focus on the rocking response of the foundation. It is certainly a simplification, which can be considered realistic for relatively slender systems, where the response is rocking-dominated. In such cases, even with a realistic friction coefficient, sliding would hardly take place, as rocking could be the critical mechanism.

The location and type of lateral (and vertical) boundaries was an important consideration. Under monotonic and cyclic static loading these boundaries can be placed fairly close to the foundation (just outside the "pressure bulb") and they can be of any "elementary" type (from "free" to "fixed"). Under dynamic loading, however, waves emanating from the footing–soil interface cannot propagate to infinity unless special transmitting boundaries are placed at suitably large distances. "Elementary" boundaries may cause spurious reflections, thereby contaminating the wave field below the foundation and reducing or even eliminating the radiation damping. For the rocking stiffness under static conditions which are the focus of this paper, "elementary" boundaries are placed at a reasonably-large distance from the foundation. In view of the fact that moment loading on the surface of a homogeneous halfspace induces normal vertical stresses which decay very rapidly in both the horizontal and the vertical direction ("pressure bulb" of limited extent: less than one-half the width from the foundation edge, in either direction—Gazetas [15]), the boundaries were placed in most cases at distances of about $\mathbf{3}\boldsymbol{B}$ from the edges of the footing. (For the plane-strain case, they were placed even farther away.)

For the total stress analysis under undrained conditions, soil behavior is modeled through a nonlinear constitutive model [4], which is a slight modification of a model incorporated in ABAQUS. It uses the Von Mises failure criterion, with yield stress σ_y related to the undrained shear strength, $\boldsymbol{S_u}$, as $\sigma_y = \sqrt{3}\,\boldsymbol{S_u}$ along with a nonlinear kinematic and isotropic hardening law, and an associative plastic flow rule. The numerical model employed herein has been validated against centrifuge and large scale physical model tests in [4]. More specifically, the "TRISEE" experiments were used to validate the model for the case of a spread footing resting on sand (not discussed herein), while centrifuge model tests conducted at UC Davis [18] were utilized for the case of clay. The latter refer to a rectangular foundation having a factor of safety against vertical loading $\boldsymbol{F_S}$=2.6, resting on a fairly homogenous layer of San Francisco Bay mud. The model was shown to capture the moment–rotation (M–ϑ) loops of the experiment (for cyclic pushover testing) for the entire range of response, from

quasi-elastic (i.e., at very small rotations), to nonlinear, and to the ultimate capacity. The numerical prediction was shown to be accurate both in terms of footing moment capacity, and with respect to the accumulated settlement during cyclic loading.

In this study, model parameters are calibrated to fit published G: γ curves of Vucetic and Dobry [53] for a plasticity index, $PI=30$. More details on the calibration procedure can be found in [4]. The performance of the numerical model was verified once more (errors less than 5%) by comparing the computed static ultimate vertical force, N_{uo}, for a strip against the classical analytical solution of Prandlt (see later). Furthermore, the initial practically-elastic rotational stiffness, $K_{R,elastic}$, of the footing (before the initiation of uplifting or soil yielding) was about 10% higher than the analytical solution.

3. Dimensionless parameters and nomenclature

A key objective of the paper is to develop solutions for the "effective" stiffness in rocking of arbitrarily-shaped foundations. In the realm of large strains we will define as "effective" stiffness of the M–ϑ response:

$$K_R = M/\vartheta \tag{1}$$

K_R depends not only on the shear modulus G, the (pertinent) footing width to the third power B^3 (or R^3), and the Poisson's ratio ν, but also on the value of the undrained shear strength S_u, and most significantly on the angle of rotation ϑ. In turn, the (effective) shear modulus G is a function of G_o (modulus at vanishingly small shear strains, γ) and the way $\Gamma \equiv G/G_o$ decreases with increasing γ. Invoking the Vaschy–Buckingham Π-theorem of dimensional analysis, the following dimensionless expression can be written:

$$\frac{K_R}{K_{R,elastic}} = f\left(\vartheta,\ \frac{N_{uo}}{N},\ \Gamma(\gamma),\ \frac{G_o}{S_u}\right) \tag{2}$$

As will be shown below, the "rigidity-index" G_o/S_u plays a rather small role for the K_R ratio. Moreover only one $\Gamma(\gamma)$ (i.e. one G/G_o versus γ) curve is utilized in this paper. Since the factor of safety against vertical loading $F_S=N_{uo}/N_u$, it can be stated that:

$$K_R = K_R(\vartheta, F_S) \tag{3a}$$

The purely elastic stiffness is thus denoted as:

$$K_{R,\ elastic} \equiv K_R(0,\infty) \tag{3b}$$

At vanishingly small angles of rotation the stiffness decreases with decreasing F_S (increased soil yielding) and thus we will have

$$K_R = K_R(0, F_S) < K_R(0,\infty) \tag{3c}$$

while, eventually, at larger angles of rotation:

$$K_R = K_R(\vartheta, F_S) < K_R(0, F_S) \tag{3d}$$

We will express:

$$K_R(\vartheta, F_S) = K_R(0, F_S)\chi(\vartheta) = K_{R,\ elastic}\psi(F_S)\chi(\vartheta) \tag{4}$$

4. Elastic stiffness

At very small angles of rotation ϑ, linear elasticity describes soil behavior while tension can be sustained at the underside of the foundation (thanks to the vertical superimposed load). Closed-form expressions for the moment–rotation ratios (stiffnesses), $K_{R,elastic}$, of surface footings are available in the literature for a variety of shapes [10,16,31,36,48,49,52,54] as follows (referring to the case of pure moment):

- Strip footing of width $B=2b$ (per unit length):

$$K_{R,\ elastic} = \frac{\pi}{2}\ \frac{G\,b^2}{1-\nu} \tag{5}$$

- Circular footing of radius R:

$$K_{R,\ elastic} = \frac{8}{3}\ \frac{G\,R^3}{1-\nu} \tag{6}$$

- Square footing of side $B=2b$:

$$K_{R,\ elastic} = 3.65\ \frac{G\,b^3}{1-\nu} \tag{7}$$

- Rectangular footing of width $B=2b$ (normal to the x direction) and length $L=2l$ (normal to the y direction). Rotation about the x axis (as in Fig. 1):
  If $B<L$:

$$K_{R,\ elastic} = 0.62\ \frac{G\,b^3}{1-\nu}\ (1+5\,l/b) \tag{8}$$

  If $B \geq L$ (as is the rectangle studied here):

$$K_{R,\ elastic} = 3.72\ \frac{G\,b^3}{1-\nu}\ (l/b)^{0.60} \tag{9}$$

It is worthy to note that using numerical (e.g., finite-element) discretization to derive these stiffnesses would most likely lead to differences of up to 10–20%, depending on the type and size of the finite elements, and on the treatment of the interface (frictionless, versus perfectly adhesive, versus Coulomb-frictional).

5. Ultimate (plastic) response

At somewhat larger values of ϑ, soil response becomes nonlinear once shear strains, γ, exceed a threshold (of the order of 0.02%) that is a function mainly of the clay plasticity index [29,53]. Thereafter, with further increasing ϑ the footing behavior depends strongly on the available factor of safety (F_S), defined as the ratio N_{uo}/N_u, where N_{uo}=the bearing capacity under purely vertical static loading, and N_u=the applied vertical load.

The ultimate moment resistance to foundation rotation is a function of the vertical (normal) force and the horizontal (shear) force, acting on the foundation. It has become popular to predict undrained ultimate limit states under a general combination of N, Q, M explicitly and to represent the collapse loads as a failure envelope in the 3-dimensional N_u, Q_u, M_u coordinate system. Whereas rigorous limit analysis solutions are available only for strip and circular foundations, the finite element method has been used successfully to produce ultimate states for rectangular shapes [6,21,23–25,27,41,47,50]. An important finding of research published in the last five years is that the shape of the failure envelope is independent of the footing shape [24,25]. In our particular case, where no lateral displacement is allowed to develop and hence the arising shear force is negligibly small (although not exactly zero, due to a "parasitic" rotation–shear coupling), the failure envelope in M_u, N_u coordinates is a parabola. For rectangular (in plan) footings, of width B and length L, Gourvenec [24] has shown that when the N_u and M_u axes are normalized by N_{uo} and N_{uo} B, respectively, a unique failure

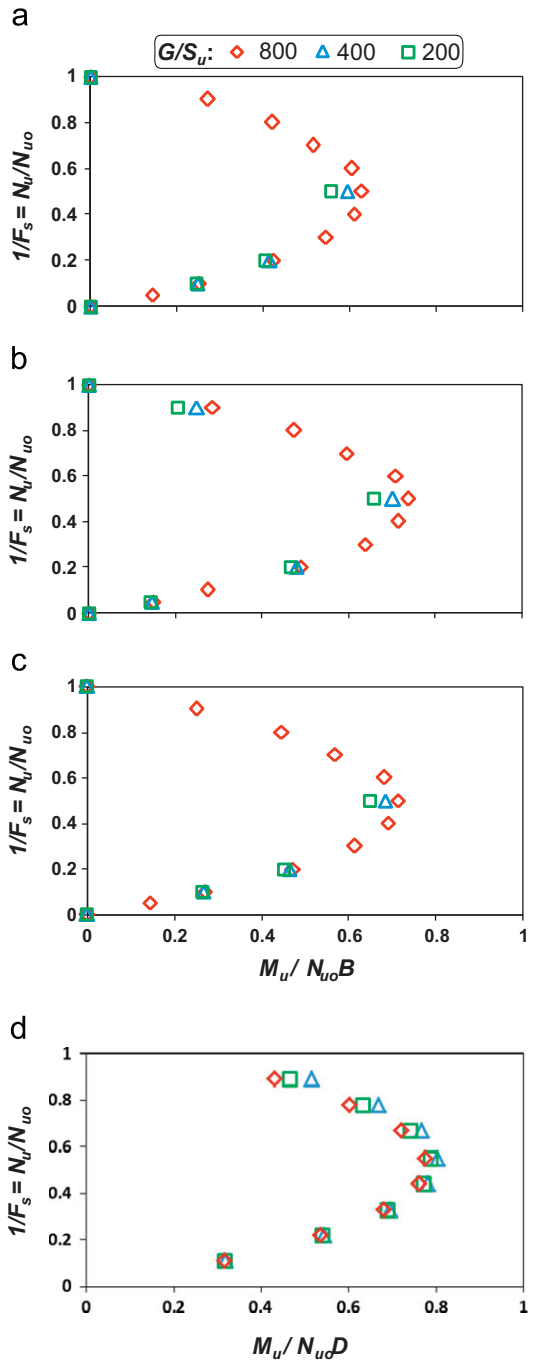

Fig. 3. Moment capacity with respect to the safety factor against vertical loading for the examined foundation geometries: (a) strip, (b) square, (c) rectangular (3:1), and (d) circular.

envelope is obtained, independent of the aspect ratio, B/L, where $B<L$. The Gourvenec envelope is given in Fig. 4.

We obtained the failure envelopes under combined vertical and moment loading, i.e., in $\boldsymbol{M_u}$, $\boldsymbol{N_u}$ space, using a finite-element discretization such as that of Fig. 2 for four foundation shapes: the strip $(B/L=0)$ and square $(B/L=1)$ which were also part of the Gourvenec unique envelope, but also the circle (radius R) and a narrow rectangle of $B/L=3$ (typical of foundations of shear walls). Note that in this paper $\boldsymbol{B}$ is always the width of the side normal to the axis of rotation (i.e. the width of the most significant side)—in this case $\boldsymbol{x}$.

The ($\boldsymbol{M_u}$, $\boldsymbol{N_u}$) failure envelopes for the above four footing shapes (strip, square, circle, elongated rectangle) are portrayed in Fig. 3. The abscissa is invariably $\boldsymbol{N_u/N_{uo}}$. The ordinate is $\boldsymbol{M_u/S_u AB}$, where $\boldsymbol{A}$ is the soil–footing contact area and $\boldsymbol{B}$ is the width of the footing side normal to the axis of rotation. Of all the problem parameters that were investigated only the "rigidity" index, $\boldsymbol{G_o/S_u}$, seems to have some effect on the peak values of the normalized failure envelope. As $\boldsymbol{G_o/S_u}$ changes from 800 to 200 the $\boldsymbol{max\ M_u}$ decreases by 10%—a rather insignificant effect which will be neglected in the sequel.

An alternative normalization of the ultimate moment, $\boldsymbol{M_u}$, is achieved by dividing it by $\boldsymbol{N_{uo}\ B}$. The following $\boldsymbol{N_{uo}}$ analytical–experimental established expressions [24,25,41,47,50] have been utilized:

- Strip ($\boldsymbol{B}$, ∞), per unit length,

$$\boldsymbol{N_{uo}=(\pi+2)S_uB} \tag{10}$$

- Square (B, B)

$$\boldsymbol{N_{uo}\approx(\pi+3)S_uB^2} \tag{11}$$

- Circle ($D=2R$)

$$\boldsymbol{N_{uo}=6.05\ S_u\ \pi\ D^2} \tag{12}$$

- Rectangle (B, $3B$)

$$\boldsymbol{N_{uo}\approx 1.065(\pi+2)S_u(3B^2)} \tag{13}$$

The results of this new normalization fall within a very narrow band, defining the unique parabola:

$$\boldsymbol{M_u/N_{uo}B\approx 0.55(N_u/N_{uo})(1-N_u/N_{uo})} \tag{14}$$

which exceeds by just 10% the classical results of Meyerhof [41]. (See also Gourvenec [24].). Interestingly, the largest moment capacity, $\boldsymbol{M_u\approx 0.14\ N_uB}$ is somewhat higher than the classical $\boldsymbol{M_u=0.125\ N_{uo}B}$, achieved for $\boldsymbol{N_u/N_{uo}}=0.5$, i.e. when the static factor of safety against vertical bearing capacity failure, $\boldsymbol{F_S=N_{uo}/N_u}=2$. The performance of the FE models is considered satisfactory, as the difference with the classical solution (i.e., the error) is of the order of 10%.

6. Nonlinear stiffness

If soil exhibited linearly-elastic ideally-plastic behavior, the above solutions based on elasticity and plasticity would be sufficient to describe the monotonic response of the foundation. Soil nonlinearity, however, develops well before the foundation–soil system reaches its ultimate moment capacity $\boldsymbol{M_u}$. A convenient popular way of displaying such nonlinearity is with the shear-modulus and damping versus shear–strain curves, such as the ones from Vucetic and Dobry [53] and Ishibashi and Zhang [29]. In fact, two phenomena take place before the ultimate capacity is reached:

- soil nonlinearities first appear at relatively small strain levels, γ, of the order of 10^{-4};
- detachment from the soil and hence uplifting of the edge of the footing takes place, as no attraction can develop between the two media in contact.

It turns out that lightly loaded foundations, with $\boldsymbol{F_S=N_{uo}/N}$ well in excess of 2, experience partial uplifting from the supporting ground before any substantial nonlinearity develops in the soil. In contrast, heavily loaded foundations, with $\boldsymbol{F_S}$ of about 2 or less, will

exhibit the opposite trend: development of strongly inelastic soil response with subsequent minor uplifting, or even no uplifting at all. Eventually, heavily and lightly loaded foundations will mobilize failure mechanisms in the soil, and thereafter the moment–rotation curve will reach its plateau. (Reference is made to [2–4,7–9,13,14,17, 26,35,42,45,46,51] for additional information.)

Fig. 5 illustrates the different failure mechanisms at incipient collapse (i.e., just before overturning) of a footing subjected to displacement-controlled monotonic pushover loading, while carrying three different vertical loads $N=N_u<N_{uo}$. The corresponding three vertical factors of safety are: $F_S=20$ (very-lightly loaded foundation, or very hard soil), $F_S=2$ (rather heavily-loaded foundation, or moderately-stiff soil); and $F_S=1.2$ (severely-loaded foundation, or quite soft soil). The three snapshots (all at incipient collapse) show vividly that as F_S decreases the extent of uplifting diminishes, but soil inelasticity increases. The extent (in both vertical and horizontal direction) of the failure zone increases substantially with a reduction in F_S, approaching the extent of failure under purely vertical loading.

Fig. 5 (top) illustrates the phases of foundation response in terms of moment–rotation ratio for the three types of foundation vertical loading: $F_S\approx$ **1.25**, **2.0**, and **20**. Notice that despite the largest elastic stiffness of the $F_S=20$ footing, its ultimate moment capacity is the smallest. This should not surprise the reader: as can be seen in Fig. 4, as $F_S\to\infty$, i.e. $N_u/N_{uo}\to 0$, M_u tends to vanish due to the inability of the tensionless interface to sustain any moment in the absence of vertical load. A convenient way of utilizing results such as those of Fig. 5 is by obtaining the **secant modulus** as a function of the amplitude of the angle of rotation, for each value of F_S.

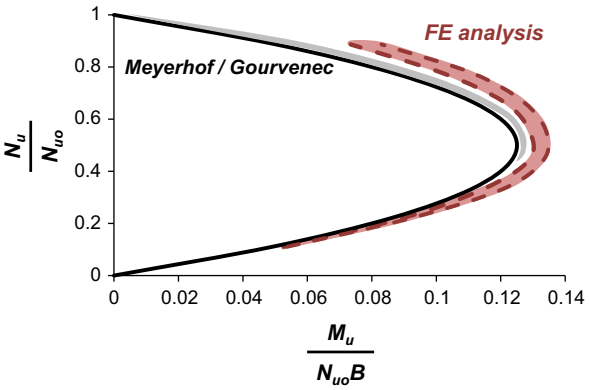

Fig. 4. Comparison of our FE analysis with the published failure envelope of Gourvenec [24] for various B/L ratios and combined M–N loading: normalized moment capacity as a function of normalized vertical load. The solid bold line corresponds to the unique envelope from the classical solution of Meyerhof [41].

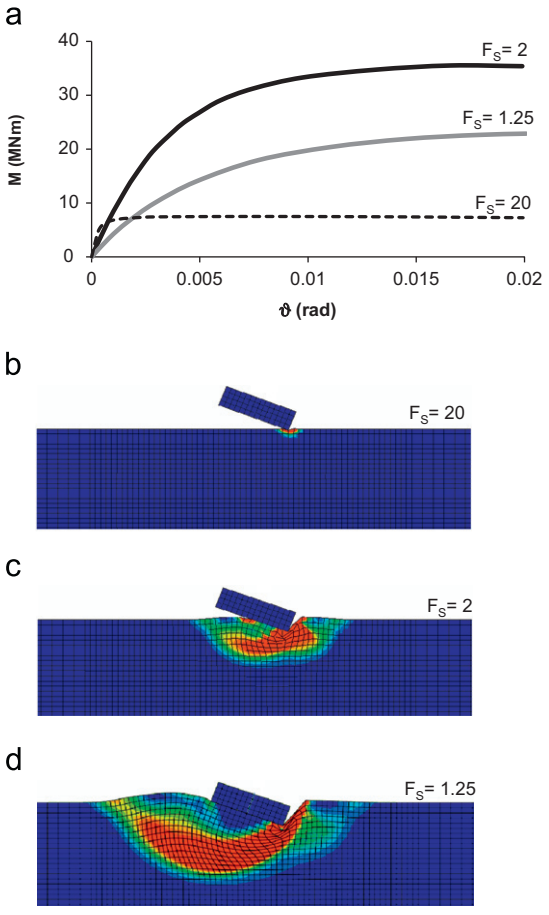

Fig. 5. Example of a footing subjected to displacement-controlled moment loading: (a) moment–rotation (M–ϑ) response for three different factors of safety against vertical bearing failure: F_s=20, 2, and 1.25; Snapshots of deformed mesh with superimposed plastic strain contours for : (b) F_s=20, (c) F_s=2, and (d) F_s=1.25.

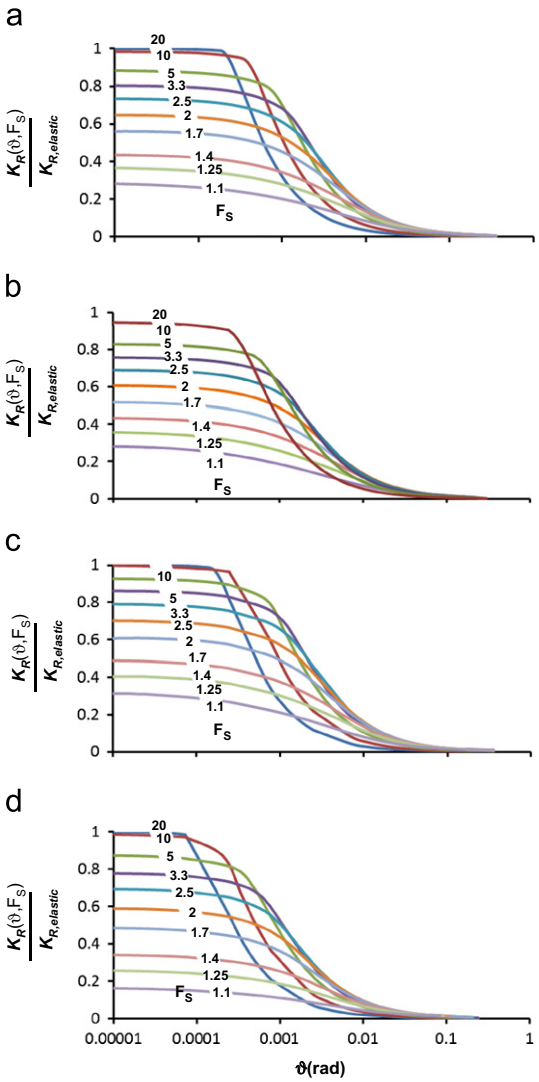

Fig. 6. Dimensionless rotational stiffness with respect to rotation amplitude and safety factor against vertical loading for the four examined foundation geometries: (a) strip, (b) square, (c) circular, and (d) rectangular (3:1).

Fig. 6 (a–d) present the K_R curves for each of the four foundation plans (circle, strip, square, 3:1 rectangle, respectively). K_R has been normalized by the corresponding $K_{R,elastic}$ value from Eqs. (5)–(7),(9). Two trends are worthy of note: **(i)** that the initial value of the ratio decreases with decreasing F_S—an obvious consequence of the unavoidable nonlinearities in the soil stemming from the increasingly-"heavy" vertical loading; and **(ii)** the rate of decrease of K_R with increasing amplitude of rotation is higher for the footings with the higher F_S—a result of the dominant role of uplifting in the case of lightly-loaded footings.

Motivated by the success of the normalization for the ultimate M_uN_u envelope, we have come by trial and error to the following normalization of the axes of the above K_R–ϑ diagrams. The objective was to derive results that, for each value of F_S, would be nearly unique for all footing shapes. By "nearly unique" we mean that the results fall within a relatively narrow band, and thus could be generalized and used in practice with any foundation shape.

Specifically, K_R is divided by K_R $(0, F_S)$ instead of by $K_{R,\ elastic}$. Using the values of the diagrams in Fig. 6 and defining

$$\psi = \psi(F_S) = K_R(0,F_S)/K_{R,\ elastic} \tag{15}$$

the following simple expression of ψ as a function of the N/N_{uo} ratio is fitted to the data:

$$\psi \approx 1 - 0.8/F_S \tag{16}$$

The angle of rotation ϑ is normalized by a characteristic value, ϑ_S, the expression of which (developed below) is motivated by the angle which initiates separation and uplifting of the footing corner from the soil: ϑ_{uplift}. Specifically:

(a) For a footing of **any shape on a rigid base**, the overturning moment initiating uplift is simply:

$$M_{uplift,\ R} = \frac{N\,B}{2} \tag{17}$$

where B is the width in the direction of rocking.

(b) For rocking of a strip or rectangle on *elastic halfspace:*

$$M_{uplift,\ H} \approx \frac{N\,B}{4} \tag{18}$$

and therefore,

$$\vartheta_{uplift,\ H} \approx \frac{N\,B}{4\,K_{R,\ \mathrm{elastic}}} \tag{19}$$

Interestingly, for an elastic Winkler base (i.e., assuming a linear distribution of stresses underneath the footing), the moment at incipient uplift reduces to $NB/6$ instead of $NB/4$ (i.e., 1.5 times less than on a halfspace).

(c) For a **circular** foundation of diameter $D=2R$ on **elastic halfspace**:

$$\vartheta_{uplift,\ H} \approx \frac{N\,D}{5.7\,K_{R,\ \mathrm{elastic}}} \tag{20}$$

As in the previous case, assuming a linear distribution of stresses underneath the footing, the moment at incipient uplift is $NB/8$ (i.e., roughly 1.5 times less than on a halfspace).

(d) For very heavily-loaded footings where the initial foundation settlement is substantial and the soil is already in a state of extensive widespread yielding ("plastification"), the angle of uplifting initiation is larger. Eventually, for small enough F_S, uplifting is hardly discernible in the M–ϑ curves.

As previously mentioned, the initial rotational stiffness K_R $(0, F_S)$ is a decreasing function of F_S (Eq. (16)). The decrease of F_S leads to increased soil yielding underneath the foundation (under purely vertical loading), i.e. even before application of moment loading. Hence, it is reasonable to assume that the uplift rotation will actually be a function of K_R $(0, F_S)$ instead of $K_{R,\ elastic}$. Focusing on rectangular foundations, and combining Eq. (19) with Eq. (16), a "characteristic" rotation angle ϑ_S (the equivalent of the uplift rotation for inelastic soil) can be defined and used as the normalization parameter:

$$\vartheta_S = \frac{N\,B}{4\,K_{R,\mathrm{elastic}}\,\psi(F_S)}\left[1 - 0.22\left(1-\frac{1}{F_S}\right)^2\left(\frac{B}{L}\right)^{0.2}\right] \tag{21}$$

While the first part of the expression is quite straightforward, its second part was determined heuristically (i.e., by trial and error) so that the results would fall within a relatively narrow band for all foundation shapes examined. Of course, simplicity to the extent possible was also an objective of this exercise. Especially for circular foundations, it is simply considered a reasonable simplification.

Indeed, with the above normalizations of the two axes [i.e., with $K_R(0, F_S)$ *and* ϑ_S, respectively] the results of Fig. 6 "collapse" to the nearly-unique curves (for each F_S value) plotted in Fig. 7. The deviation from the mean value for each F_S is rather insignificant, so that one could safely use these curves for any (reasonable) foundation shape (ranging from a circle to a rectangle). More complicated foundations, such as H-shaped, L-shaped, C-shaped, have not been investigated.

It is therefore proposed that such curves, along with the associated expressions presented in this paper, be used in preliminary equivalent-linear analyses of soil–foundation systems.

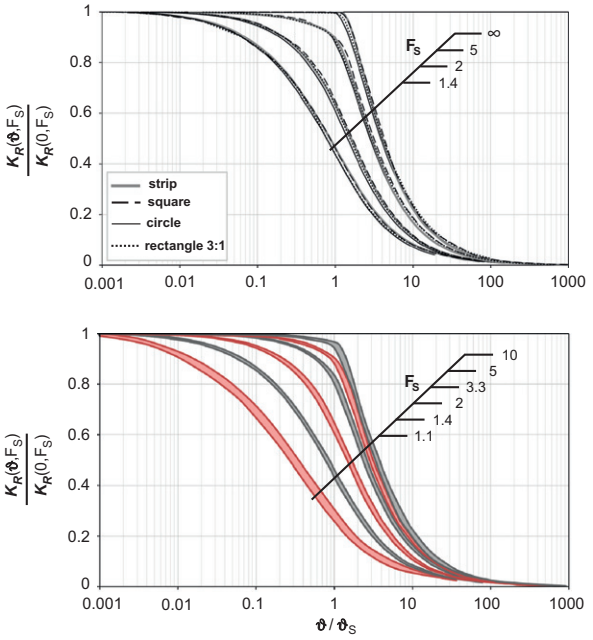

Fig. 7. Normalized rotational stiffness versus angle of rotation normalized with the characteristic angle θ_s for eight factors of safety. The upper diagram depicts in detail the results for the various footing geometries examined; the lower diagram summarizes the results for different safety factors.

7. Example application: natural period of rocking oscillator

The system shown in Fig. 8 is a rigid **1–dof** oscillator (i.e., having a fixed-base period equal to zero) of mass m at a height h, supported on stiff clay, with $S_u=150$ kPa, $G_o=90$ MPa, and $\nu=0.49$.

Because of the relatively large slenderness ratio $h/B=2$ (or $h/b=4$, for the equivalent rigid block) rocking of the foundation will be the

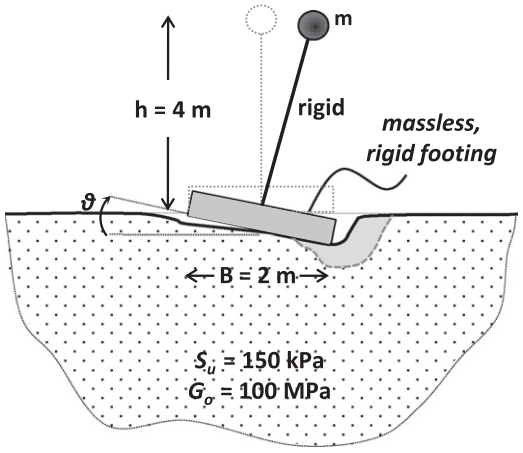

Fig. 8. Example problem definition : rigid oscillator of height $h=4$ m lying on a rigid $B=2b=2$ m square (or equivalent strip) foundation on compliant nonlinear clayey soil of $\boldsymbol{Su}=150$ kPa and $\boldsymbol{Go}=100$ Mpa.

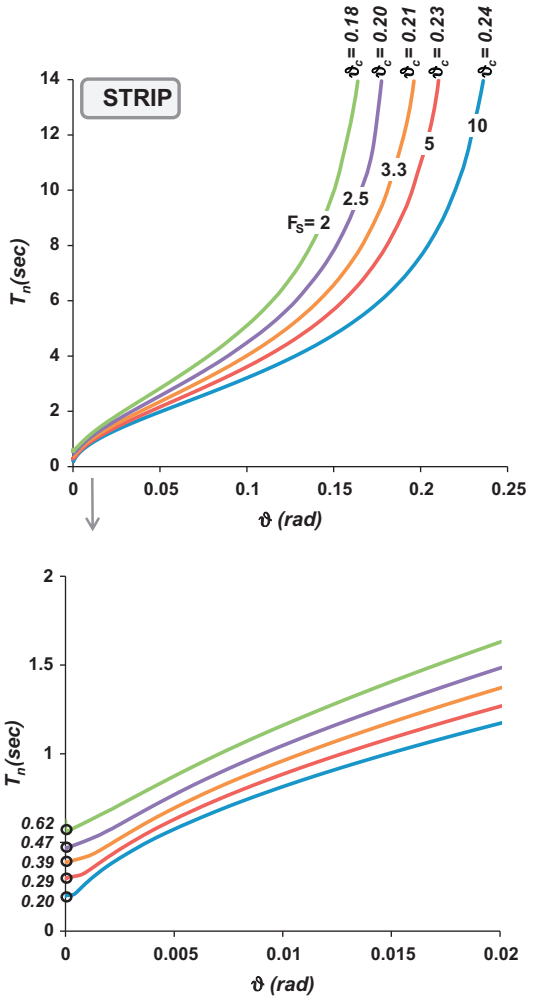

Fig. 9. Example rigid oscillator of height $h=4$ m lying on a rigid $B=2b=2$ m strip foundation on compliant nonlinear clayey soil of $\boldsymbol{S_u}=150$ kPa and $\boldsymbol{G_o}=100$ MPa: rocking period $\boldsymbol{T_n}$ as a function of rotation amplitude $\boldsymbol{\vartheta}$ for various factors of safety against vertical loading $\boldsymbol{F_s}$, for the entire rotation regime (top), and zoomed view for rotations of practical interest (bottom).

dominant mode of vibration. The system is in essence an inverted pendulum. Within the simplification of the equivalent linearization, neglecting any horizontal displacement of the footing, but accounting for P–Δ effects, the differential equation of free vibrations at not very large angles $\boldsymbol{\vartheta}$ becomes:

$$\left(\boldsymbol{m\,h^2}\right)\ddot{\boldsymbol{\vartheta}}+(\boldsymbol{K_R}-\boldsymbol{mgh})\boldsymbol{\vartheta}\approx\boldsymbol{0} \tag{22}$$

$$\boldsymbol{T_n}\approx 2\pi\sqrt{\frac{\boldsymbol{m\,h^2}}{\boldsymbol{K_R}-\boldsymbol{mgh}}} \tag{23}$$

where $\boldsymbol{K_R}=\boldsymbol{K_R}(\boldsymbol{\vartheta},\boldsymbol{F_S})$. Thus, for each value of $\boldsymbol{\vartheta}$ and of $\boldsymbol{F_S}=\boldsymbol{N_{uo}}/\boldsymbol{mg}$, a unique value of $\boldsymbol{K_R}$ is obtained. $\boldsymbol{N_{uo}}$ is given by one of the Eqs. (10)–(13).

Figs. 9 and 10 portray (for a strip and a square footing) the natural period of the oscillator $\boldsymbol{T_n}(\boldsymbol{\vartheta},\boldsymbol{F_S})$ as a function of $\boldsymbol{\vartheta}$, for five different factors of safety $\boldsymbol{F_S}$. The graphs at the bottom of each figure show in detail the initial part of the $\boldsymbol{T_n}(\boldsymbol{\vartheta},\boldsymbol{F_S})$ curves (for $\boldsymbol{\vartheta}<\boldsymbol{0.02}$, which is considered as a reasonable range for typical building structures). Several trends are noteworthy:

- The initial period (at $\boldsymbol{\vartheta}=0$) can be written as:

$$\boldsymbol{T_n}(0,\boldsymbol{F_S})\approx 2\pi\sqrt{\frac{\boldsymbol{N_{uo}\,h^2}}{\boldsymbol{F_S\,g\,K_{R,\mathrm{elastic}}}\,\boldsymbol{\psi}(\boldsymbol{F_S})}} \tag{24}$$

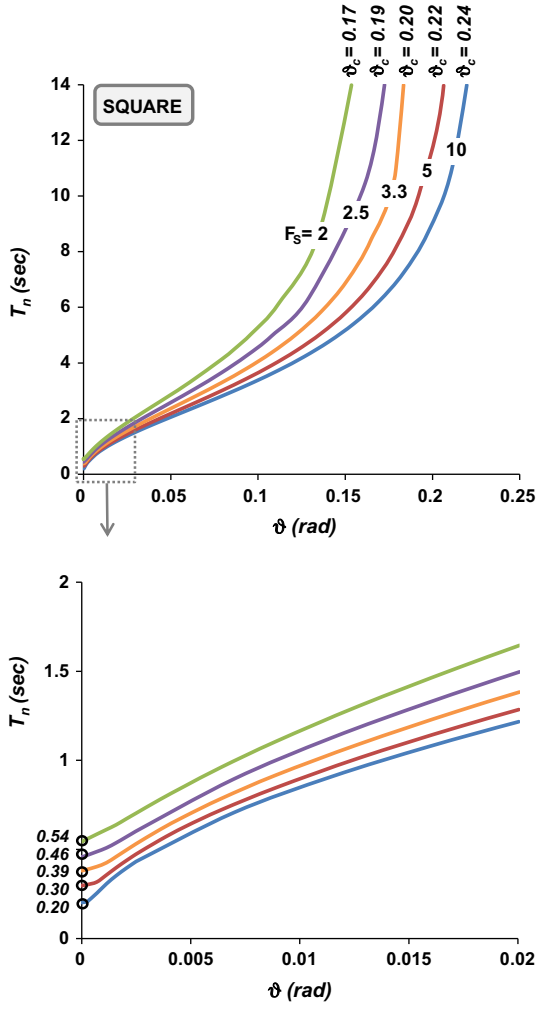

Fig. 10. Example rigid oscillator of height $h=4$ m lying on a rigid $B=2b=2$ m square foundation on compliant nonlinear clayey soil of $\boldsymbol{S_u}=150$ kPa and $\boldsymbol{G_o}=100$ MPa: rocking period $\boldsymbol{T_n}$ as a function of rotation amplitude $\boldsymbol{\vartheta}$ for various factors of safety against vertical loading $\boldsymbol{F_s}$, for the entire rotation regime (top), and zoomed view for rotations of practical interest (bottom).

As clearly seen in the enlarged bottom graphs of the two figures, and as it would be intuitively expected, $T_n(0,F_S)$ decreases with the increase of F_S. For the specific example and the F_S values considered, the periods $T_n(0,F_S)$ vary between 0.2 and 0.7 s for both footings. Quite interestingly, the shape of the footing seems to play a truly minor role.

- At relative small values of ϑ (<0.05 rad), T_n increases with ϑ almost at a constant or slightly decreasing rate. But thereafter, T_n increases exponentially, approaching asymptotically infinity at $\vartheta=\vartheta_c$, the critical angle for overturning collapse.
- This large increase in the natural period of oscillation T_n is one of the main causes of the beneficial role played by geometric nonlinearity and material inelasticity in reducing the distress of the superstructure during strong seismic shaking—an idea which has been under intensive investigation in recent years [3,4,8,14,17–20,26,32–35,38,40,46].
- For large values of F_S, ϑ_c is a purely geometric parameter:

$$\vartheta_c \approx \arctan\frac{b}{h} \approx \frac{b}{h} \tag{25}$$

In this specific example, $\vartheta_c \approx 0.245$. And ϑ_c decreases with decreasing values of F_S, i.e., as yielding in the soil becomes increasingly prevalent. The values of ϑ_c for all factors of safety F_S are obtained from Figs. 9 and 10.

8. Conclusion

Formulas and charts have been developed in a general dimensionless format which will allow easy computation of the nonlinear effective rotational stiffness of foundations of any (reasonable) shape. These results despite their numerical origin, are based on some assumptions (such as the homogeneous clay under undrained conditions) that may only crudely approximate reality. Furthermore the concept of equivalent linear analysis is only a crude approximation at conditions near failure. Despite these clearly admitted simplifications, the results presented herein would be useful for design purposes—a step forward compared to current practice of design on the basis of elastic stiffnesses.

Acknowledgment

The financial support of this work has been provided through the European Research Council (ERC) Programme "Ideas: Support of Frontier Research", under Contract number ERC–2008–AdG228254–DARE. We are thankful for this support.

References

[1] ABAQUS 6.1. Standard user's manual. Rhode Island: Hibbit, Karlsson and Sorensen, 2007.
[2] Anastasopoulos I, Gazetas G, Loli M, Apostolou M, Gerolymos N. Soil failure can be used for seismic protection of structures. Bulletin of Earthquake Engineering 2009;8(2):309–26.
[3] Anastasopoulos I. Beyond conventional capacity design: towards a new design philosophy. In: Orense RO, Chow N, Pender MJ, editors. Soil–foundation–structure interaction. New York: CRC Press, Taylor & Francis Group; 2010 p. 213–20.
[4] Anastasopoulos I, Gelagoti F, Kourkoulis R, Gazetas G. Simplified constitutive model for simulation of cyclic response of shallow foundations: validation against laboratory tests. Journal of Geotechnical and Geoenvironmental Engineering 2011;137(2):1154–68.
[5] Apostolou M, Gazetas G, Garini E. Seismic response of slender rigid structures with foundation uplifting. Soil Dynamics and Earthquake Engineering 2007;27:642–54.
[6] Butterfield R, Gottardi G. A complete three-dimensional failure envelope for shallow footings on sand. Géotechnique 1994;44(1):181–4.
[7] Chatzigogos CT, Pecker A, Salencon J. Macroelement modeling of shallow foundations. Soil Dynamics and Earthquake Engineering 2009;29(6):765–81.
[8] Chen XC, Lai YM. Seismic response of bridge piers on elastic-plastic Winkler foundation allowed to uplift. Journal of Sound and Vibration 2003;266(5):957–65.
[9] Cremer C, Pecker A, Davenne L. Modeling of nonlinear dynamic behaviour of a shallow strip foundation with macro-element. Journal of Earthquake Engineering 2002;6(2):175–211.
[10] Dobry R, Gazetas G. Dynamic response of arbitrarily–shaped foundations. Journal of Geotechnical Engineering 1986;113(2):109–35.
[11] Faccioli E, Paolucci R, Vanini M. 3D site effects and soil-foundation interaction in earthquake and vibration risk evaluation. Final Report of the European research project TRISEE, Politecnico di Milano, 1998.
[12] FEMA. Prestandard and Commentary for the Seismic Rehabilitation of Buildings. Manual no. 356, Federal Emergency Management Agency, 2000.
[13] Figini R. Nonlinear dynamic soil–structure interaction: application to seismic analysis of structures on shallow foundations. Doctoral Dissertation, Politecnico di Milano, 2010.
[14] Gajan S, Kutter BL. Effects of moment-to-shear ratio on combined cyclic load–displacement behavior of shallow foundations from centrifuge experiments. Journal of Geotechnical and Geoenvironmental Engineering 2009;135(8):1363–81.
[15] Gazetas G. Simple physical methods for foundation impedances. In: Benerjee PK, Butterfield R, editors. Dynamics of foundations and buried structures. Elsevier Applied Science, London; 1987 Chapter 2: p. 44–90.
[16] Gazetas G. Formulas and charts for impedances of surface and embedded foundations. Journal of Geotechnical Engineering 1991;117(9):1129–41.
[17] Gazetas G, Apostolou M. Nonlinear soil–structure interaction: foundation uplifting and soil yielding. In: Proceedings of the 3rd USA–Japan workshop on soil–structure interaction, 2004, Menlo Park, California.
[18] Gajan S, Phalen JD, Kutter BL, Hutchinson TC, Martin G. Centrifuge modeling of load deformation behavior of rocking shallow foundations. Soil Dynamics and Earthquake Engineering 2005;25(7–10):773–83.
[19] Gelagoti F, Kourkoulis R, Anastasopoulos I, Gazetas G. Rocking-isolated frame structures: margins of safety against toppling collapse and simplified design approach. Soil Dynamics and Earthquake Engineering 2012;32(1):87–102.
[20] Gelagoti F, Kourkoulis R, Anastasopoulos I, Gazetas G. Rocking isolation of frame structures founded on separate footings. Earthquake Engineering and Structural Dynamics 2012;41:1177–97.
[21] Georgiadis M, Butterfield R. Displacements of footings on sands under eccentric and inclined loading. Canadian Geotechnical Journal 1988;25(2):199–212.
[22] Gerolymos N, Apostolou M, Gazetas G. Neural network analysis of overturning response under near-fault type excitation. Earthquake Engineering & Engineering Vibration 2005;4(2):213–28.
[23] Gottardi G, Houlsby GT, Butterfield R. The displacement of a model rigid surface footing on dense sand under general planar loading. Soils and Foundations 1995;35(3):71–82.
[24] Gouvernec S. Shape effects on the capacity of rectangular footings under general loading. Géotechnique 2007;57(8):637–46.
[25] Gouvernec S, Randolph MF, Kingsnorth O. Undrained bearing capacity ofsquare and rectangular footings. International Journal of Geomechanics 2006;6(3):147–57.
[26] Harden CW, Hutchinson TC, Moore M. Investigation into the effects of foundation uplift on simplified seismic design procedures. Earthquake Spectra 2006;22(3):663–92.
[27] Houlsby GT, Cassidy MJ, Einav I. A generalized Winkler model for the behavior of shallow foundation. Géotechnique 2005;55(6):449–60.
[28] Housner GW. The behavior of inverted pendulum structures during earthquakes. Bulletin of Seismological Society of America 1963;53(2):403–17.
[29] Ishibashi I, Zhang X. Unified dynamic shear moduli and damping ratios of sand and clay. Soils and Foundations 1993;33(1):l12–191.
[30] Kausel E. Forced vibrations of circular foundations on layered media. Research Report R74-11, Department of Civil Engineering, Massachusetts Institute of Technology, 1974.
[31] Kausel E, Roesset JM. Dynamic stiffness of circular foundations. Journal of the Engineering Mechanics Division 1975;101:771–85.
[32] Kawashima K, Nagai T, Sakellaraki D.. Rocking seismic isolation of bridges supported by spread foundations. In: Proceedings of 2nd Japan–Greece workshop on seismic design, observation, and retrofit of foundations, Tokyo, Japanese Society of Civil Engineers, 2007, p. 254–65.
[33] Koh AS, Spanos P, Roesset JM. Harmonic rocking of rigid block on flexible foundation. Journal of Engineering Mechanics 1986;112(11):1165–80.
[34] Kourkoulis R, Anastasopoulos I, Gelagoti F, Kokkali P. Dimensional analysis of SDOF systems rocking on inelastic soil. Journal of Earthquake Engineering 2012;16(7):995–1022.
[35] Kutter BL, Martin G, Hutchinson TC, Harden C, Gajan S, Phalen JD. Workshop on modeling of nonlinear cyclic load–deformation behavior of shallow foundations. Report of PEER Workshop, University of California, Davis, 2003.
[36] Luco JE, Westman RA. Dynamic response of circular footings. Journal of the Engineering Mechanics Division 1971;97(5):1381–95.
[37] Makris N, Roussos Y. Rocking response of rigid blocks under near source ground motions. Géotechnique 2000;50(3):243–62.

[38] Martin GR, Lam P. Earthquake resistant design of foundations: retrofit of existing foundations. In: Proceedings of the geo-engineering 2000 conference, Melbourne, Australia, 2000, state-of-the art paper.
[39] Meek J. Effect of foundation tipping on dynamic response. Journal of Structural Division 1975;101(7):1297–311.
[40] Mergos PE, Kawashima K. Rocking isolation of a typical bridge pier on spread foundation. Journal of Earthquake Engineering 2005;9(2):395–414.
[41] Meyerhof GG.. The bearing capacity of foundations under eccentric and inclined loads. In: Proceedings of the 3rd international conference of soil mechanics and foundation engineering, Zurich, 1953, vol. 1, p. 440–5.
[42] Panagiotidou AI.. 2D and 3D inelastic seismic response analysis of foundation with uplifting and P–Δ effects. Diploma thesis, National Technical University, Athens, 2010.
[43] Paolucci R. Simplified evaluation of earthquake induced permanent displacement of shallow foundations. Journal of Earthquake Engineering 1997;1(3): 563–79.
[44] Paolucci R, Pecker A. Seismic bearing capacity of shallow strip foundations on dry soils. Soils and Foundations 1997;37:95–105.
[45] Paolucci R, Shirato M, Yilmaz MT. Seismic behavior of shallow foundations shaking table experiments vs numerical modeling. Earthquake Engineering & Structural Dynamics 2008;37:577–95.
[46] Pecker A. Influence of nonlinear soil structure interaction on the seismic demand of bridges. In: Proceedings of the international conference on innovations on bridges and soil bridge interaction, published by Eugenides Foundation, Athens, Greece, 2011, p. 91–106.
[47] Randolph MF, Puzrin AM. Upper bound limit analysis of circular foundations on clay under general loading. Géotechnique 2003;53(9):785–96.
[48] Roesset JM. Stiffness and damping coefficients of foundations. In: O' Neil MW, Dobry R, editors. Dynamic response of foundations: analytical aspects. ASCE, New York; 1980 p. 1–30.
[49] Roesset JM. The use of simple models in soil-structure interaction. Civil Engineering and Nuclear Power 1980;1:1–25.
[50] Salençon J, Pecker A. Ultimate bearing capacity of shallow foundations under inclined and eccentric loads. Part II: Purely cohesive soil without tensile strength. European Journal of Mechanics-A/Solids 1995;14(3):377–96.
[51] Shirato M, Kouno T, Nakatani S, Paolucci R. Large-scale model tests of shallow foundations subjected to earthquake loads. In: Proceedings of the 2nd Japan–Greece workshop on seismic design, observation, and retrofit of foundations, Japanese Society of Civil Engineers, Tokyo, 2007, p. 275–99.
[52] Vetetsos AS, Wei YT. Lateral and rocking vibration of footings. Journal of the Soil Mechanics and Foundation Division 1971;97:1227–48.
[53] Vucetic M, Dobry R. Effect of soil plasticity on cyclic response. Journal of Geotechnical Engineering 1991;117(1):89–107.
[54] Wolf JP. Soil–structure interaction analysis in time-domain. Englewood Cliffs, N.J.: Prentice–Hall; 1988.